# The effects of contaminating noise on the calculation of active acoustic intensity for pressure gradient methods

Mylan R. Cook, Kent L. Gee, Tracianne B. Neilsen, and Scott D. Sommerfeldt

Citation: The Journal of the Acoustical Society of America **145**, 173 (2019); doi: 10.1121/1.5084046
View online: https://doi.org/10.1121/1.5084046
View Table of Contents: https://asa.scitation.org/toc/jas/145/1
Published by the Acoustical Society of America

# The effects of contaminating noise on the calculation of active acoustic intensity for pressure gradient methods

Mylan R. Cook,[a] Kent L. Gee, Tracianne B. Neilsen, and Scott D. Sommerfeldt
*Department of Physics and Astronomy, Brigham Young University, N283 ESC Provo, Utah 84602, USA*

(Received 17 September 2018; revised 19 November 2018; accepted 27 November 2018; published online 9 January 2019)

Bias errors for two-dimensional active acoustic intensity using multi-microphone probes have been previously calculated for both the traditional cross-spectral and the Phase and Amplitude Gradient Estimator (PAGE) methods [Whiting, Lawrence, Gee, Neilsen, and Sommerfeldt, J. Acoust. Soc. Am. **142**, 2208–2218 (2017)]. Here, these calculations are expanded to include errors due to contaminating noise, as well as probe orientation. The noise can either be uncorrelated at each microphone location or self-correlated; the self-correlated noise is modeled as a plane-wave with a varying angle of incidence. The intensity errors in both magnitude and direction are dependent on the signal-to-noise ratio (SNR), frequency, source properties, incidence angles, probe configuration, and processing method. The PAGE method is generally found to give more accurate results, especially in direction; however, uncorrelated noise with a low SNR (below 10–15 dB) and low frequency (wavelengths more than 1/4 the microphone spacing) can yield larger errors in magnitude than the traditional method—though a correction for this is possible. Additionally, contaminating noise does not necessarily impact the possibility of using the PAGE method for broadband signals beyond a probe's spatial Nyquist frequency. 
https://doi.org/10.1121/1.5084046

[KGS] Pages: 173–184

## I. INTRODUCTION

Intensity is an important acoustic measure and is useful for applications such as source characterization and localization. Acoustic source characterization in real-world environments can be subject to inaccuracies caused by contaminating noise, whether acoustic, fluid mechanical (e.g., wind) or electrical. These inaccuracies extend to vector acoustic intensity calculations made from pressure measurements obtained with multiple-microphone probes. Intensity, or more specifically active acoustic intensity, is the time-averaged energy flux density. For a given frequency and location, it is a vector-valued quantity that describes the magnitude and direction of the propagating acoustic energy. Accurate estimates of both complex pressure and particle velocity are necessary because intensity is calculated with their product.[1]

Traditionally, acoustic intensity has been calculated using a multi-microphone processing method developed in the 1970s known as the *p-p* method or finite difference method.[1–4] This method—which is referred to here as the traditional method—estimates the pressure gradient by taking finite sums and differences of the real and imaginary components of the frequency domain complex pressures. The intensity is therefore calculated by using cross-spectral values from the microphones on the intensity probe. Another processing method available is the phase and amplitude gradient estimator (PAGE) method.[2,5] Instead of using the real and imaginary components of the complex pressures, it uses the magnitude and phase components. The intensity in this case is calculated using auto-spectral values and the arguments of cross-spectral values.[5–8] Because of differences between the traditional and PAGE methods, the calculated intensity can vary depending on which method is used.

In order to compare the effectiveness of these two methods, calculated intensity can be compared to the known analytical intensity to find the bias errors. A bias error gives a measure of the difference between analytical solutions and the values obtained by using a specific processing method. These errors can depend on many different factors. Previous work has shown how different bias errors are obtained for various probe geometries for both methods using either a plane-wave source or a monopole source.[8–10]

These previous studies are now expanded to investigate the effects contaminating noise and probe rotation have on the bias errors. The effects of both correlated and uncorrelated contaminating noise are investigated for single probe geometry, followed by a summary of the effects of using different probe geometries. In general, the PAGE method has lower bias errors in the calculated intensity direction than the traditional method, and in most cases the intensity magnitude bias errors are lower as well. However, for low-level signals at low frequencies, the traditional method may yield a better intensity calculation. In general, the traditional method has larger bias errors than the PAGE method at higher frequencies (wavelengths less than 1/4 the microphone spacing), and also when self-correlated noise is present.

## II. METHODOLOGY

The active acoustic intensity $\boldsymbol{I}$ at a point is calculated in the frequency domain as

[a]Electronic mail: mylan.cook@gmail.com.

$$\boldsymbol{I} = \frac{1}{2}\mathrm{Re}\{p\boldsymbol{u}^*\}, \tag{1}$$

where $p$ is the complex pressure, $\boldsymbol{u}$ is the vector complex particle velocity, and Re indicates the real part. (Bold letters indicate vector quantities and * indicates complex conjugation.) By using Euler's equation, the complex particle velocity can be obtained from the gradient of the complex pressure as

$$\boldsymbol{u} = \frac{j}{\omega\rho_0}\nabla p, \tag{2}$$

where $j$ is the imaginary unit, $\omega$ is the angular frequency, and $\rho_0$ is the fluid density. Accurate calculation of the intensity therefore depends upon an accurate calculation of the pressure gradient, as well as the pressure. The two processing methods calculate the pressure gradient differently, which leads to different bias errors.

For probe configurations where the intensity is calculated in two dimensions, the bias errors—the difference between the analytical intensity, $\boldsymbol{I}$, and the calculated intensity, $\boldsymbol{I}_{\mathrm{calc}}$—consist of a magnitude error and an angular error, defined, respectively, as

$$L_{\epsilon,\boldsymbol{I}} = 10\log_{10}\left(\frac{|\boldsymbol{I}_{\mathrm{calc}}|}{|\boldsymbol{I}|}\right)\mathrm{dB}, \tag{3}$$

$$\theta_{\epsilon,\boldsymbol{I}} = \theta_{\mathrm{calc}} - \theta, \tag{4}$$

where $\theta$ and $\theta_{\mathrm{calc}}$ are the directions of $\boldsymbol{I}$ and $\boldsymbol{I}_{calc}$ as polar angle in the plane of the probe, respectively. Perfect calculation would yield $L_{\epsilon,\boldsymbol{I}} = 0$ dB and $\theta_{\epsilon,\boldsymbol{I}} = 0°$. Previous studies[6] have shown how these bias errors differ in an ideal, noiseless field where the source is located at a specific angular location relative to the probes investigated. Expanding upon this work, the effects of both probe orientation and contaminating noise present in the sound field are taken into consideration.

When trying to localize or characterize acoustic sources of interest, the presence of contaminating noise introduces several additional variables to bias error calculations. Though independent of the source of interest, the contaminating noise can either be uncorrelated or self-correlated at the microphone probe location, e.g., an extraneous acoustic signal that arrives at a specified angle relative to the probe, yielding a specific phase relationship for the noise itself. In practice, it is possible for the contaminating noise to fall between these two extremes, being partially self-correlated. Both the degree of correlation and the relative amplitude of the signal to the contaminating noise amplitude, or the signal-to-noise ratio (SNR), will further affect the bias errors.

The bias errors vary with frequency. The traditional method has an upper frequency limit—known as the spatial Nyquist frequency $f_N$, which is the frequency at which the microphone spacing is equal to 1/2 of a wavelength—above which intensity results are not considered valid.[9] The PAGE method can be used above $f_N$ for broadband signals with the use of phase unwrapping.[11] Though frequencies above $f_N$ are not discussed in this paper, the equations for the bias errors for the PAGE method—with a broadband source and broadband noise—remain valid up to frequencies at which probe scattering effects must be taken into account, so long as phase unwrapping can be performed correctly. When phase values do not exhibit jumps of more than $\pi$ radians between frequency bins, phase unwrapping is trivial. For narrowband sources, low-level additive broadband noise can actually improve estimation of intensity above $f_N$ with the PAGE method, so long as certain conditions are met; these results will be presented in a forthcoming paper, as only frequencies below $f_N$ are investigated herein.

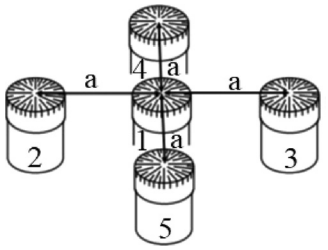


FIG. 1. A five-microphone orthogonal probe. The microphones are numbered 1 to 5, and in the $x$-$y$ plane of the probe—where $\hat{x}$ goes from 1 to 3 and $\hat{y}$ goes from 1 to 4—have positions (0,0), (-a,0), (a,0), (0,a), and (0,-a), respectively.

The remainder of this paper addresses the effects of extraneous noise on the bias errors from the calculation of active intensity using the traditional and PAGE methods. Section III of this paper deals with uncorrelated noise using a five-microphone orthogonal probe, pictured in Fig. 1. This probe was chosen as it has a center microphone to directly measure the pressure, as well as two pairs of orthogonally positioned microphones, which can be used to test for symmetry. For this probe, $f_N$ is reached when $ka = \pi$, where $k$ is the wavenumber and $a$ is the microphone probe radius. Section IV deals with self-correlated or plane-wave-like (directional constant-amplitude) noise with the same probe geometry. Different probe geometries are discussed in Sec. V with regard to both correlated and uncorrelated noise. The reason for using $a$ as the probe radius rather than simply the microphone spacing is for comparison of different probe geometries with the same overall probe dimensions. Equations for all of the cases described can be found in Tables V–IX in the Appendix.

## III. BIAS ERRORS CAUSED BY UNCORRELATED CONTAMINATING NOISE

In the frequency domain, the total complex pressure at microphone $\mu$ is obtained by summing the pressure due to the source and the pressure due to the contaminating noise,

$$p_\mu = p_{s_\mu} + p_{n_\mu} = A_{s_\mu}e^{-jk\phi_{s_\mu}} + A_{n_\mu}e^{-jk\phi_{n_\mu}}, \tag{5}$$

where $A$ is the pressure amplitude, $\phi$ is the phase, and the subscripts $s$ and $n$ indicate source and contaminating noise, respectively. If the complex pressure due to the contaminating noise exhibits a position-dependent relationship in phase and magnitude, e.g., equal amplitude at each position and phase differences proportional to the distance between

microphones, the noise is said to be correlated. When no such relationship exists, the noise is uncorrelated.[12] Some examples of uncorrelated noise are electrical noise in the microphone and data acquisition system or pressures at the level of the noise floor.

Using the pressure measurements from the microphones, the auto- and cross-spectral values—needed to calculate the intensity—can be obtained using the procedure laid out in Sec. 6.1.3 of Bendat and Piersol[12] as, respectively,

$$G_{\mu\mu} = G_{s_\mu s_\mu} + G_{s_\mu n_\mu} + G_{n_\mu s_\mu} + G_{n_\mu n_\mu}, \tag{6}$$

$$G_{\mu\nu} = G_{s_\mu s_\nu} + G_{s_\mu n_\nu} + G_{n_\mu s_\nu} + G_{n_\mu n_\nu}. \tag{7}$$

Using the ensemble average, the individual terms are given by

$$G_{\mu\nu} = \begin{cases} p_\mu p_\nu^* & \text{for correlated signals } \mu \text{ and } \nu \\ 0 & \text{for uncorrelated signals } \mu \text{ and } \nu. \end{cases} \tag{8}$$

Because the contaminating noise is uncorrelated with the source, all cross terms between the source and contaminating noise are zero. For the cross spectrum, because the noise is itself uncorrelated at different locations, $G_{n_\mu n_\nu}$ is also zero using ensemble averaging. Though uncorrelated noise does not necessarily exhibit any specific amplitude relationship, it is reasonable to assume—especially for relatively compact probes and well-matched microphones—that the SNR is equal at each microphone position, so $A_{n_\mu} = A_{n_\nu} \equiv A_n$. The auto-spectral and cross-spectral values can then be simplified to give

$$G_{\mu\mu} = A_{s_\mu}^2 + A_n^2, \tag{9}$$

$$G_{\mu\nu} = A_{s_\mu} A_{s_\nu} e^{-jk(\phi_{s_\mu} - \phi_{s_\nu})}. \tag{10}$$

### A. Plane-wave source

The first source considered is a plane-wave, for which the amplitude at each microphone location is the same, so $A_{s_\mu} = A_{s_\nu} \equiv A_s$. The plane-wave propagates with an angle $\theta_s$ with respect to the positive $x$ axis or $\hat{x}$, as the probe coordinates in Fig. 1 have been defined. This results in auto- and cross-spectral values such as

$$G_{11} = \cdots = G_{55} = A_s^2 + A_n^2, \tag{11}$$

$$G_{12} = A_s^2 e^{jka\cos\theta_s}. \tag{12}$$

The analytical result for the intensity caused by a plane-wave of amplitude $A_s$ in the absence of contaminating noise is

$$\boldsymbol{I} = \frac{A_s^2}{2\rho_0 c}\cos\theta_s\hat{x} + \frac{A_s^2}{2\rho_0 c}\sin\theta_s\hat{y} = \frac{A_s^2}{2\rho_0 c}\hat{\theta}_s, \tag{13}$$

where $c = \omega/k$ is the sound speed.

Using Eq. (13), the formulas for calculating the orthogonal components of the intensity bias, $I_{\hat{x}}$ and $I_{\hat{y}}$, can be found in Table V in the Appendix (which also includes other probe configurations, discussed further on). The total bias errors are then given by

$$L_{\epsilon,\boldsymbol{I}} = 10\log_{10}\left(\sqrt{I_{\hat{x}}^2 + I_{\hat{y}}^2}\right) = 5\log_{10}(I_{\hat{x}}^2 + I_{\hat{y}}^2), \tag{14}$$

$$\theta_{\epsilon,\boldsymbol{I}} = \tan^{-1}\left(\frac{I_{\hat{y}}}{I_{\hat{x}}}\right) - \theta_s. \tag{15}$$

All equations given are complete, but are dependent upon several independent variables. Therefore, in order to present and interpret the results in a concise manner, the absolute value of the bias errors is averaged across all angles of incidence $\theta_s$, and this average bias error is used for the following figures. This averaging allows results to be presented as only a function of $ka$ and SNR, where $\text{SNR} = 10\log_{10}(A_s^2/A_n^2)$. In many cases this averaging does not have a large effect, though for complete results the equations in the tables in the appendix should be used, rather than just looking at the figures—most notably this averaging can obscure the effect of probe rotation very near a monopole source. It should be noted that for the traditional method, as $ka$ approaches $f_N$ the intensity magnitude is usually underestimated rather than overestimated,[8] so—since the absolute value is used—the bias errors give how much the traditional method under-calculates the intensity. Conversely, contaminating noise usually causes the PAGE method to calculate a larger value for the intensity than the analytic solution, so the bias errors give this over-calculated value.

Since the traditional method calculates the intensity using weighted cross-spectra, and since uncorrelated noise terms cancel out in cross-spectral values, the bias errors for the traditional method here are independent of SNR (see Table I). As such—and due to the averaging across all angles of incidence—the magnitude and bias errors are plotted as only a function of $ka$ in Fig. 2. Though uncorrelated noise does not affect the bias errors for the traditional method, larger errors are seen for large values of $ka$ (above 0.5), which illustrate the bandwidth limitation of the traditional method.

Unlike the traditional method, the PAGE method calculates intensity using weighted auto-spectra and the arguments of cross-spectra. Because of this, the bias errors depend heavily on the SNR, but are independent of $ka$ when the phase can be unwrapped correctly (see Table I). Note also that the magnitude and angular portions of the bias errors are entirely separable—the magnitude bias depends on the auto-spectral values, while the angular bias depends on cross-spectral values, and the total bias is the product of the two. Additionally, for this case the bias errors are independent of the angle of incidence, so the averaging is redundant. The results are seen in Fig. 3, and are plotted as a function of SNR.

Interestingly, for an incident plane-wave and uncorrelated contaminating noise there is no angular bias incurred by using the PAGE method, as seen in Fig. 3(b). This accuracy is because the intensity is computed by using the arguments of cross-spectra, for which uncorrelated noise cancels out, and due to the separable nature of the magnitude and angle errors. For a plane-wave source with uncorrelated contaminating noise, the PAGE method computes the direction perfectly regardless of frequency, microphone spacing, SNR, or angle of incidence.

The magnitude bias errors for the PAGE method are very predictable, and depend solely upon SNR, as seen in Fig. 3(a).

TABLE I. Orthogonal intensity bias components and bias errors for a plane-wave source and uncorrelated noise. Similar equations for other probe geometries are given in Table VI.

| Plane-wave source uncorrelated noise | | |
|---|---|---|
| | Traditional | PAGE |
| $I_{\hat{x}}$ | $\frac{\sin(ka\cos\theta_s)}{ka}$ | $(1+10^{(-\mathrm{SNR}/10)})\cos\theta_s$ |
| $I_{\hat{y}}$ | $\frac{\sin(ka\sin\theta_s)}{ka}$ | $(1+10^{(-\mathrm{SNR}/10)})\sin\theta_s$ |
| $L_{\epsilon,\boldsymbol{I}}$ | $5\log_{10}\left(\left(\frac{\sin(ka\cos\theta_s)}{ka}\right)^2+\left(\frac{\sin(ka\sin\theta_s)}{ka}\right)^2\right)$ | $10\log_{10}(1+10^{(-\mathrm{SNR}/10)})$ |
| $\theta_{\epsilon,\boldsymbol{I}}$ | $\tan^{-1}\left(\frac{\sin(ka\sin\theta_s)}{\sin(ka\cos\theta_s)}\right)-\theta_s$ | 0 |

The increase in sound pressure level, and therefore the bias, is singularly dependent on the additional squared pressure due to the contaminating noise. Because of this, there is a doubling of pressure from the noiseless case, or a rise of 3 dB, when the SNR approaches zero.[16] For large SNR values, the magnitude error asymptotically approaches zero as expected.

Because the magnitude bias is so predictable and independent of (the zero-valued) angular bias, a simple correction can be used to scale the PAGE intensity magnitude appropriately using the SNR or the coherence. The coherence between microphone pairs can be calculated using the auto-spectral and cross-spectral values; for the plane-wave source, it is identical for each microphone pair and is

$$\gamma_{\mu\nu}^2=\frac{|G_{\mu\nu}|^2}{G_{\mu\mu}G_{\nu\nu}}=\frac{1}{\left(1+\frac{A_n^2}{A_s^2}\right)^2}=\frac{1}{(1+10^{-\mathrm{SNR}/10})^2}. \quad (16)$$

The square root of the coherence is the correction factor needed to account for the presence of the uncorrelated noise,

$$\sqrt{\gamma_{\mu\nu}^2}=\frac{1}{1+10^{-\mathrm{SNR}/10}}. \quad (17)$$

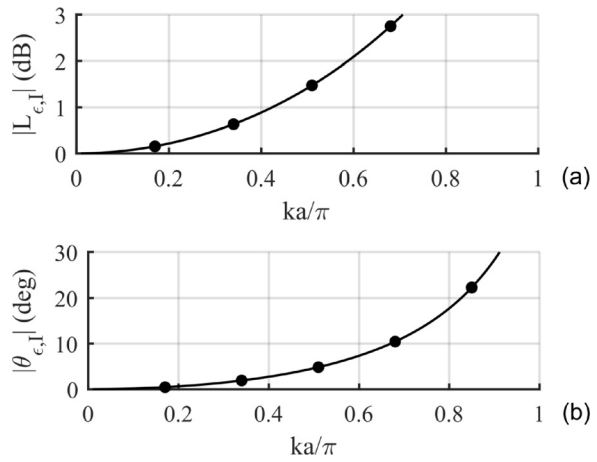


FIG. 2. Traditional method bias errors in (a) the magnitude and (b) the direction of the active intensity calculated for a plane-wave source with uncorrelated contaminating noise using a five-microphone orthogonal probe. The bias errors are plotted as a function of only $ka$ because the results are independent of SNR and are averaged across all possible angles of incidence.

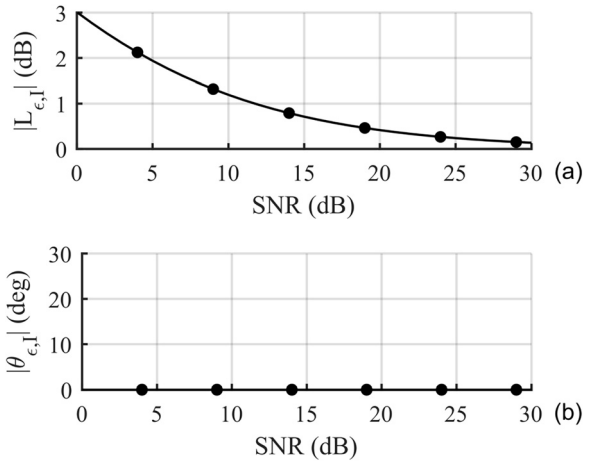


FIG. 3. PAGE method bias errors in (a) the magnitude and (b) the direction of the active intensity calculated for a plane-wave source with uncorrelated contaminating noise. This method is dependent on SNR but independent of $ka$. Note the horizontal axis is different than that in Fig. 2. Traditional method bias errors in (a) the magnitude and (b) the direction of the active intensity calculated for a plane-wave source with uncorrelated contaminating noise using a five-microphone orthogonal probe. The bias errors are plotted as a function of only $ka$ because the results are independent of SNR and are averaged across all possible angles of incidence.

If this scaling factor is multiplied by the computed intensity before it is converted to a decibel value—or equivalently a corresponding dB value can be subtracted from the computed intensity level—then $L_{\epsilon,\boldsymbol{I}}$ for the PAGE method would be zero for any SNR. Since the magnitude and angular parts are separable, this scaling factor would have no adverse effects on the calculation of the angle. This correction works perfectly for a plane-wave source with contaminating uncorrelated noise, and may be useful for other source and contaminating noise situations;[13–15,17,18] this correction will be explored in connection with a forthcoming coherence-based PAGE calculation method.

With or without correction, the PAGE method computes the correct intensity angle for a plane-wave source with uncorrelated noise, regardless of the values for $ka$, SNR, or angle of incidence. For low SNR values and very low $ka$ values, the traditional method can better estimate the intensity level; however, the magnitude obtained by the PAGE method can be corrected to obtain zero magnitude error. It is also useful to note that for broadband sources, the results for the PAGE method are the same for frequencies above $f_N$, with phase unwrapping of the transfer function applied.[11]

### B. Monopole source

For a monopole sound source, the pressure amplitude is inversely proportional to the distance $r$ between the source and the position of interest. By representing the monopole amplitude with the complex magnitude $\tilde{A}$, and letting $A_s^2=|\tilde{A}|^2/r^2$, the analytical solution is

$$\boldsymbol{I}=\frac{|\tilde{A}|^2}{2\rho_0 c r^2}\hat{\theta}_s=\frac{A_s^2}{2\rho_0 c}\hat{\theta}_s. \quad (18)$$

The auto-spectral value for microphone 1 and the cross-spectral value between microphones 1 and 2 due to the monopole source with uncorrelated contaminating noise are then

TABLE II. Intensity bias error components for a monopole source with uncorrelated noise. The bias errors $L_{\epsilon,\boldsymbol{I}} = 5\log_{10}(I_{\hat{x}}^2 + I_{\hat{y}}^2)$ and $\theta_{\epsilon,\boldsymbol{I}} = \tan^{-1}(I_{\hat{y}}/I_{\hat{x}}) - \theta_s$ are not given explicitly here since they do not easily simplify. Equations for other probe geometries are given in Table VII.

| Monopole source uncorrelated noise | | |
|---|---|---|
| | Traditional | PAGE |
| $I_{\hat{x}}$ | $\frac{\sin\left(kr - kr\sqrt{1-2\beta\cos\theta_s+\beta^2}\right)}{2ka\sqrt{1-2\beta\cos\theta_s+\beta^2}} - \frac{\sin\left(kr - kr\sqrt{1+2\beta\cos\theta_s+\beta^2}\right)}{2ka\sqrt{1+2\beta\cos\theta_s+\beta^2}}$ | $(1+10^{(-\mathrm{SNR}/10)})\left(\frac{1}{2\beta}\sqrt{1+2\beta\cos\theta_s+\beta^2} - \frac{1}{2\beta}\sqrt{1-2\beta\cos\theta_s+\beta^2}\right)$ |
| $I_{\hat{y}}$ | $\frac{\sin\left(kr - kr\sqrt{1-2\beta\sin\theta_s+\beta^2}\right)}{2ka\sqrt{1-2\beta\sin\theta_s+\beta^2}} - \frac{\sin\left(kr - kr\sqrt{1+2\beta\sin\theta_s+\beta^2}\right)}{2ka\sqrt{1+2\beta\sin\theta_s+\beta^2}}$ | $(1+10^{(-\mathrm{SNR}/10)})\left(\frac{1}{2\beta}\sqrt{1+2\beta\sin\theta_s+\beta^2} - \frac{1}{2\beta}\sqrt{1-2\beta\sin\theta_s+\beta^2}\right)$ |

$$G_{11} = \frac{|\tilde{A}|^2}{r^2} + A_n^2 = A_s^2 + A_n^2, \tag{19}$$

$$G_{12} = \frac{|\tilde{A}|^2 e^{jka\cos\theta_s}}{r^2 - ra\cos\theta_s} = \frac{A_s^2 e^{jka\cos\theta_s}}{1 - \frac{a}{r}\cos\theta_s} \equiv \frac{A_s^2 e^{jka\cos\theta_s}}{1-\beta\cos\theta_s}. \tag{20}$$

Similar auto- and cross-spectral expressions can be given for the other microphone pairs. To simplify the results, the variable $\beta$ is defined such that $\beta \equiv a/r = ka/kr$, which can take on any value between zero and one. In the near field of the monopole, as $\beta \to 1$, the bias errors are very different from the far field, where $\beta \to 0$ and the solutions converge to those of a plane-wave source. The resulting intensity components are found in Table II.

The meaning of the SNR for a monopole source is slightly different than that for a plane-wave source, since the SNR depends on the distance between a monopole source and the probe. This means that the SNR for the monopole source is the SNR at the probe location. For the monopole source, $\mathrm{SNR} = 10\log_{10}(A_s^2/A_n^2) = 10\log_{10}(|\tilde{A}|^2/r^2A_n^2)$, which is dependent on $r$. This means that if the probe were to physically be moved away from the source, the source amplitude would have to be increased—or the noise amplitude would need to be decreased—to maintain the same SNR. In practice since the source amplitude is rarely known, the SNR is usually defined at a given location.

For the monopole source with uncorrelated noise, the traditional method is still independent of SNR, and therefore identical to the noiseless case presented previously by Ref. 8. As the value of $\beta$ decreases, the bias errors no longer increase monotonically, which can be seen in Fig. 4. The magnitude bias is greater for small values of $ka$ (below about 0.5), beyond even 3 dB when $\beta \to 1$. Interestingly, the increase caused by larger $ka$ values appears later than for the plane-wave source; for some intermediate values of $ka$ the total bias actually decreases. The trends for the angular bias are the same, with an angular bias of nearly 10° for small $ka$ values (below 0.5) as $\beta \to 1$; see Fig. 4(b).

For the PAGE method, the bias errors for the monopole source are still independent of $ka$ but must be averaged across the angle of incidence as is done with the traditional

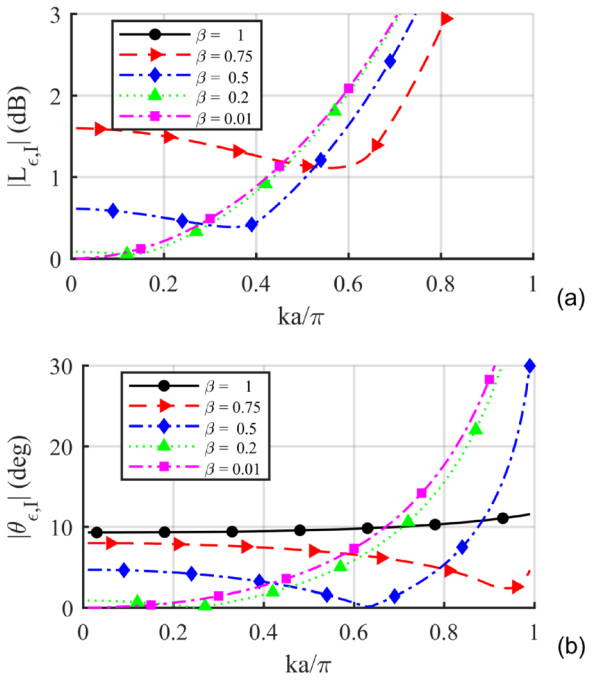


FIG. 4. (Color online) Traditional method bias errors in (a) the magnitude and (b) the direction of the active intensity calculated for a monopole source with uncorrelated contaminating noise using a five-microphone orthogonal probe. Results are averaged across angle of incidence. In (a) the bias errors for $\beta = 1$ are greater than 3 dB for all values of $ka$.

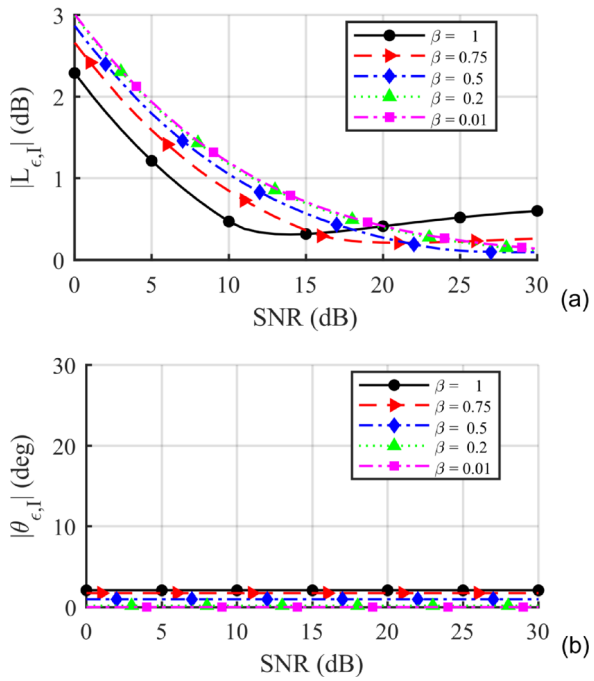


FIG. 5. (Color online) PAGE method bias errors in (a) the magnitude and (b) the direction of the active intensity calculated for a monopole source with uncorrelated contaminating noise using a five-microphone orthogonal probe, averaged across angle of incidence.

TABLE III. Intensity components for a plane-wave source with correlated noise. The total bias errors for magnitude and direction are $L_{\epsilon,\boldsymbol{I}} = 5\log_{10}(I_{\hat{x}}^2 + I_{\hat{y}}^2)$ and $\theta_{\epsilon,\boldsymbol{I}} = \tan^{-1}(I_{\hat{y}}/I_{\hat{x}}) - \theta_s$. Equations for other probe geometries are given in Table VIII.

| Plane-wave source correlated noise | | |
|---|---|---|
| | Traditional | PAGE |
| $I_{\hat{x}}$ | $\frac{\sin(ka\cos\theta_s)}{ka} + 10^{(-\mathrm{SNR}/10)}\frac{\sin(ka\cos\theta_n)}{ka}$ | $(1+10^{(-\mathrm{SNR}/10)})\frac{1}{2ka}\arg\{e^{2jka\cos\theta_s} + 10^{(-\mathrm{SNR}/10)}e^{2jka\cos\theta_n}\}$ |
| $I_{\hat{y}}$ | $\frac{\sin(ka\sin\theta_s)}{ka} + 10^{(-\mathrm{SNR}/10)}\frac{\sin(ka\sin\theta_n)}{ka}$ | $(1+10^{(-\mathrm{SNR}/10)})\frac{1}{2ka}\arg\{e^{2jka\sin\theta_s} + 10^{(-\mathrm{SNR}/10)}e^{2jka\sin\theta_n}\}$ |

method. The angular error is constant over SNR as in the plane-wave case, though non-zero; as $\beta \to 1$ the angular error approaches approximately 2°, as seen in Fig. 5(b). For small SNR values (less than about 10 dB), the PAGE method intensity magnitude errors are actually decreased slightly as $\beta$ increases, seen in Fig. 5(a). For higher SNR values (above 10 dB), however, these errors are increased slightly—this is a product of averaging across all angle of incidence. As $\beta \to 1$, the actual bias errors can show a large variance across angle of incidence. For a more complete representation, the equations in Table VII should be used. Generally, biases are larger for $\theta_s \approx 0°$ than for $\theta_s \approx 45°$.

Moving close to a monopole source has a greater effect on the traditional method than it does on the PAGE method. The PAGE method is again better for computing the intensity angle, though is not perfect and can be offset by about 2°. The magnitude offset from the plane-wave case is within about 0.7 dB for all SNR values. For the traditional method at low $ka$ values, the magnitude can be offset by more than 3 dB, and the angular offset can be near 10°.

## IV. BIAS ERRORS CAUSED BY SELF-CORRELATED CONTAMINATING NOISE

Turning now to self-correlated noise, which is still assumed to be uncorrelated with the source, the problem becomes more complicated. Assuming the contaminating noise source is not close to the probe (within a few wavelengths), the noise can be assumed to be plane-wave-like (directional, amplitude-constant) in nature. However, this plane-wave noise comes from a specific direction, $\theta_n$, and can have a very large impact on bias errors. This additional variable is not a problem when dealing with equations, though it does create additional difficulties when trying to illustrate results. Objectively averaging across possible noise directions is not possible. Instead, an angular separation $\theta_{\mathrm{sep}}$ between the source and noise directions can be defined such that $\theta_{\mathrm{sep}} = |\theta_s - \theta_n| \leq 180°$. Results can then be averaged across the angle of incidence to obtain the bias errors as a function of $ka$, SNR, and angular separation.

As now shown for both plane-wave and monopole sources, the traditional method is most sensitive to the value of $ka$ and the PAGE method is most dependent on the SNR. However, neither is completely independent of the other variable, and both depend heavily on the separation angle.

### A. Plane-wave source

For an incident plane-wave source of interest and contaminating plane-wave noise—uncorrelated with the source—the more complicated impact of correlated noise is immediately apparent from the equations in Table III. There are more independent variables, and the angular and magnitude portions are now entangled for both methods. Figures for the bias errors are presented, but can only capture a portion of the big picture.

The traditional method is not very adept at dealing with correlated noise. Figure 6(a) shows the bias errors as a function of separation angle, $\theta_{\mathrm{sep}}$, and $ka$ value for a few representative SNR values. With a large SNR, the expected errors for large $ka$ values are easily seen. With lower SNR values, there is a trade-off between magnitude and angular accuracy as the separation angle changes. For $\theta_{\mathrm{sep}} \approx 0°$ there is no angular error—again for small $ka$ values (less than 0.5) only—but a large magnitude error. For larger separation angles, the magnitude is more accurately calculated, while the angular error is larger. For large values of $ka$ both the magnitude and angular errors are extreme.

The PAGE method does not cause any bias error whenever the SNR exceeds about 20 dB, as shown in Fig. 6(b). For lower SNR values the direction can still be computed fairly accurately, most especially when there is enough phase information to obtain the correct phase gradient, i.e., for larger values of $ka$. The magnitude errors are a bit more complicated. For low values of $ka$ there is more dependence on the separation angle than there is for larger values of $ka$. For any given separation angle, the magnitude and angular calculation is better for a larger SNR value, as seen in Fig. 6(b).

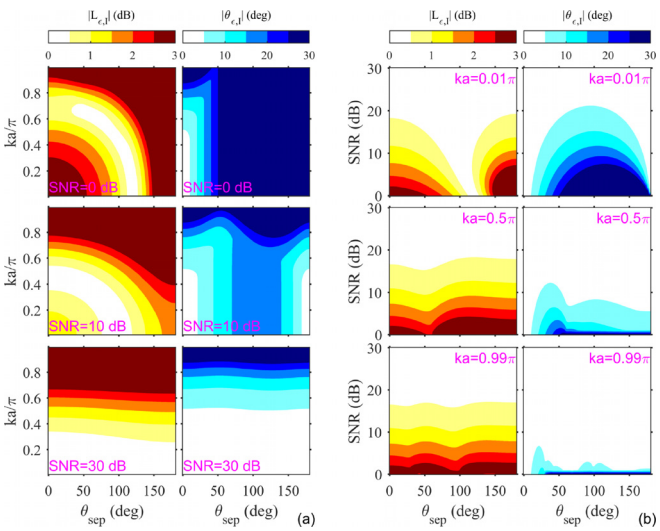


FIG. 6. (Color online) Bias errors for a plane-wave source with contaminating correlated noise using (a) the traditional method and (b) the PAGE method.

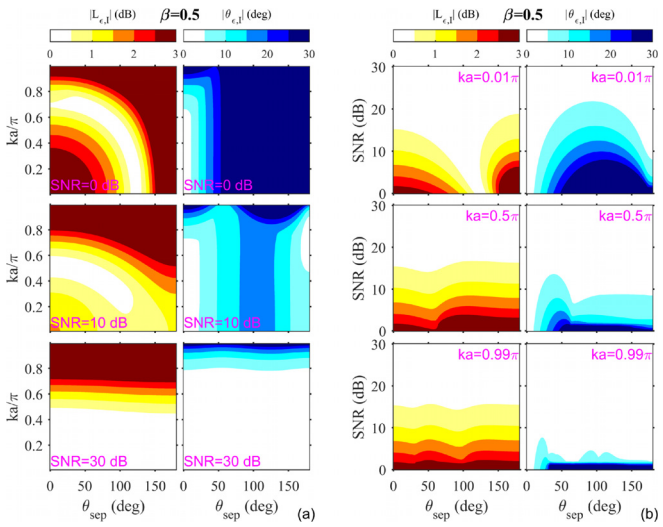


FIG. 7. (Color online) Bias errors for a monopole source located a distance $r = 2a[\beta = (ka/kr) = 0.5]$ from the probe center with contaminating correlated noise using (a) the traditional method and (b) the PAGE method.

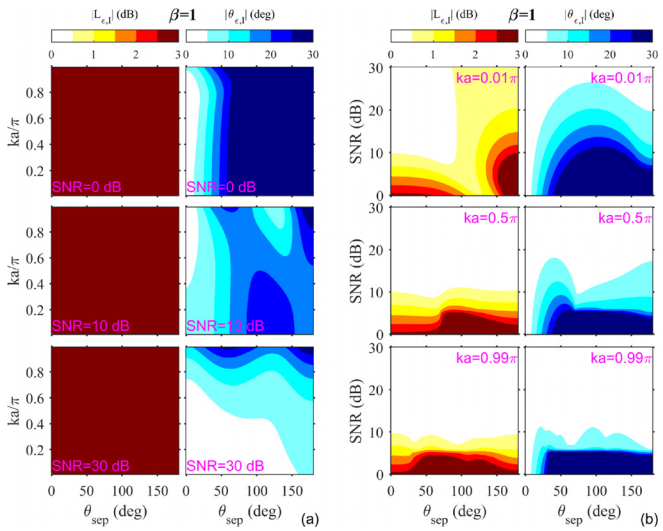


FIG. 8. (Color online) Bias errors for a monopole source located a distance $r = a\,[\beta = (ka/kr) = 1]$ from the probe center with contaminating correlated noise using (a) the traditional method and (b) the PAGE method.

The PAGE method is less dependent on separation angle than the traditional method. For low $ka$ values and low SNR values (SNR near zero), both methods show similar errors. However, for the plane-wave source with plane-wave noise, the PAGE method outperforms the traditional method as either $ka$ increases or, most especially, as the SNR increases.

### B. Monopole source

Results are again separated for the monopole source based upon the value of $\beta$, as done in Sec. III. For the sake of brevity, results for only two values of $\beta$ are portrayed—one near the source and the other as close to the monopole source as possible—in Figs. 7 and 8, while the intensity values are given in Table IV. As $\beta \to 0$, the monopole source errors approach those of the plane-wave source.

Both methods are seen to exhibit significant errors in the near field (as $\beta \to 1$) of a monopole with plane-wave noise. The PAGE method is better at computing the magnitude for all but the lowest SNR values, below a value of around 10 dB, depending on the separation angle. As $\beta \to 1$, the PAGE method clearly outperforms the traditional method for positive SNR values.

In terms of angular error, both methods behave similarly for small values of $ka$ (below 0.5) and small SNR values. For an SNR above about 10 dB the bias errors for the PAGE method are much smaller than those for the traditional method, regardless of the value of $ka$. The PAGE method can perform better at higher $ka$ values because the phase gradient can be calculated more accurately—even with noise present. For small values of $ka$, even small amounts of noise can lead to inaccurate phase gradient calculation.

## V. THE EFFECTS OF PROBE GEOMETRY

Previous results were given for specific five-microphone orthogonal probe geometry, since the probe symmetry with orthogonal pairs made the equations for the bias errors relatively simple. However, different probes can be used to calculate intensity, and each probe can estimate the pressure gradient—or the central pressure when there is no microphone in the center—differently, leading to different bias errors. Two other two-

TABLE IV. Intensity components for a monopole source with uncorrelated noise. The total bias errors are $L_{\epsilon,\boldsymbol{I}} = 10\log_{10}(\sqrt{I_{\hat{x}}^2 + I_{\hat{y}}^2})$ and $\theta_{\epsilon,\boldsymbol{I}} = \tan^{-1}(I_{\hat{y}}/I_{\hat{x}}) - \theta_s$. Equations for other probe geometries are given in Table IX.

Monopole source correlated noise

| | Traditional | PAGE |
|---|---|---|
| $I_{\hat{x}}$ | $\frac{\sin\left(kr - kr\sqrt{1-2\beta\cos\theta_s+\beta^2}\right)}{2ka\sqrt{1-2\beta\cos\theta_s+\beta^2}} - \frac{\sin\left(kr - kr\sqrt{1+2\beta\cos\theta_s+\beta^2}\right)}{2ka\sqrt{1+2\beta\cos\theta_s+\beta^2}}$ $+10^{(-\mathrm{SNR}/10)}\frac{\sin(ka\cos\theta_n)}{ka}$ | $\left(1+10^{(-\mathrm{SNR}/10)}\right)\frac{1}{2ka} * \arg\{e^{jkr(\sqrt{1+2\beta\cos\theta_s+\beta^2}-\sqrt{1-2\beta\cos\theta_s+\beta^2})}$ $+10^{(-\mathrm{SNR}/10)}\sqrt{1-2\beta^2\cos 2\theta_s+\beta^4}\,e^{2jka\cos\theta_n}\}$ |
| $I_{\hat{y}}$ | $\frac{\sin\left(kr - kr\sqrt{1-2\beta\sin\theta_s+\beta^2}\right)}{2ka\sqrt{1-2\beta\sin\theta_s+\beta^2}} - \frac{\sin\left(kr - kr\sqrt{1+2\beta\sin\theta_s+\beta^2}\right)}{2ka\sqrt{1+2\beta\sin\theta_s+\beta^2}}$ $+10^{(-\mathrm{SNR}/10)}\frac{\sin(ka\sin\theta_n)}{ka}$ | $\left(1+10^{(-\mathrm{SNR}/10)}\right)\frac{1}{2ka} * \arg\{e^{jkr(\sqrt{1+2\beta\sin\theta_s+\beta^2}-\sqrt{1-2\beta\sin\theta_s+\beta^2})}$ $+10^{(-\mathrm{SNR}/10)}\sqrt{1+2\beta^2\cos 2\theta_s+\beta^4}\,e^{2jka\sin\theta_n}\}$ |

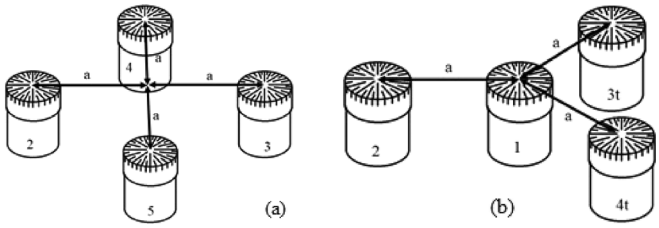


FIG. 9. Two alternate probe geometries that can be used to calculate intensity. The four-microphone orthogonal probe (a) is referred to as $4_O$ and the four-microphone triangular probe (b) is referred to as $4_T$. The five-microphone orthogonal probe in Fig. 1 is referred to as $5_O$. Note there is no microphone 1 for $4_O$, and are numbered 2 through 5 to match the numbering for $5_O$.

dimensional probe geometries, for which noiseless bias errors were previously investigated,[6] are considered herein.

By removing the center microphone from the probe seen in Fig. 1, the four-microphone orthogonal probe seen in Fig. 9(a) can be obtained. The bias errors obtained can differ largely from the results seen in Secs. III and IV, while in other cases are exactly the same. The main reason for the differences is that instead of obtaining the pressure at the center microphone directly, an average must be computed to obtain the approximate pressure at the probe center. When the pressure does not vary rapidly, this averaging does not cause significant adverse effects, but near a monopole sources the differences can be drastic. Additionally, when using the traditional method, the effective microphone spacing is now twice what it was for the five microphone probe, so $f_N$ is now reached at $ka = \pi/2$ instead of $ka = \pi$. Note that the effective doubling in microphone spacing for this probe is simply a result of not having a center microphone—the probe radius is still the same.

The third probe of interest consists of a center microphone surrounded by three microphones in an equilateral triangle configuration, each separated from the center microphone by a distance $a$. Since there is a center microphone, this probe generally works better than the four microphone orthogonal probe. For the sake of brevity, only the most significant differences caused by probe geometry are presented. The five microphone probe will hereafter be referred to as $5_O$, the four microphone orthogonal probe as $4_O$, and the four microphone triangular probe as $4_T$.

### A. Uncorrelated noise

For the traditional method, $4_O$ and $5_O$ perform similarly with two noted differences (which can be seen in Fig. 10). First, since $4_O$ has effectively double the microphone spacing of $5_O$, the bias errors are reached at 1/2 the value of $ka$. Second, very near a monopole source, $4_O$ must estimate the center pressure, yielding larger errors.

Using the traditional method with a plane-wave source, $4_T$ is identical to $5_O$ in calculating the magnitude, but can better calculate the intensity direction, seen in Fig. 10(a). Near a monopole source, $4_T$ is worse at calculating both the direction and magnitude of the intensity, seen in Figs. 10(b) and 10(c). This is due to the effective microphone spacing in orthogonal directions being $3a/2$ and $\sqrt{3}a/2$, so the random incidence average shows great variability. As $\beta = 1$, when

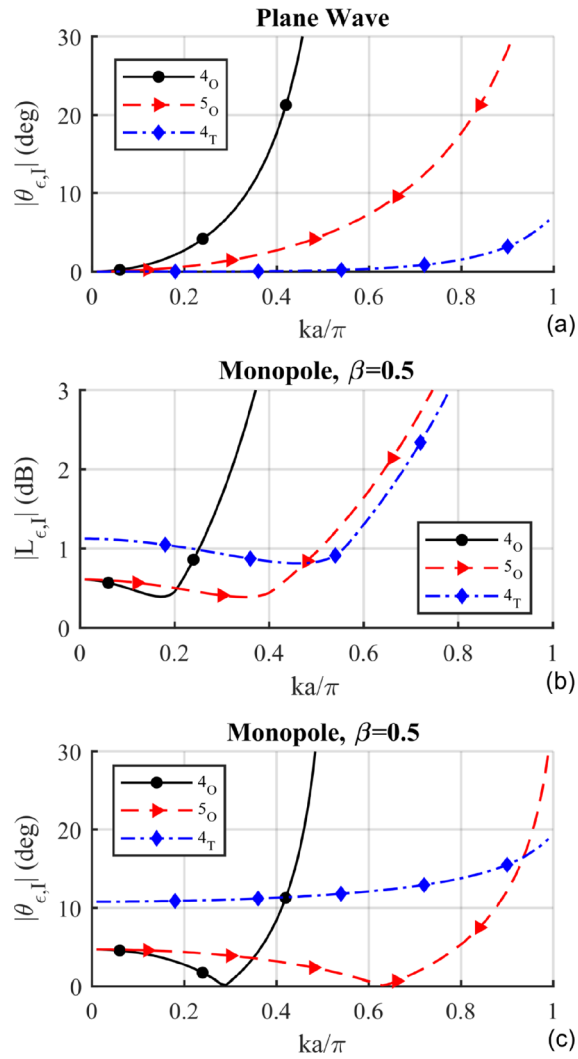


FIG. 10. (Color online) Bias errors for different probe geometries with contaminating uncorrelated noise using the traditional method. Only cases where the different probe geometries exhibit marked differences are pictured. The angular error for a plane-wave source with uncorrelated noise is given in (a), while (b) shows the magnitude error and (c) shows the angular error for a monopole source.

the probe is as close to the source as possible, the bias errors all exceed 3 dB with large angular errors.

For the PAGE method, the results for each probe configuration are exactly the same for a plane-wave source with uncorrelated noise, and so are not shown. In the near field of a monopole ($\beta \approx 1$), however, the probes give noticeably different results. Probe $5_O$ is much better at estimating the angle. This improvement results from having four microphones to calculate the angle with another mic at the center, while $4_T$ has only three for the angle. Probe $4_O$ has to estimate the center pressure, making it the least effective of the three probe geometries at calculating the intensity direction. With regard to magnitude, $4_O$ is very inaccurate, again due to the lack of a direct center pressure measurement. Whether the bias errors for $4_T$ are less than or greater than those for $5_O$ depends on the value of $\beta$ and the SNR. These results can be seen in Fig. 11. Again note that for $\beta \approx 1$, averaging across angle of incidence provides an incomplete representation. Biases are larger for $\theta_s \approx 0°$ than for $\theta_s \approx 45°$.

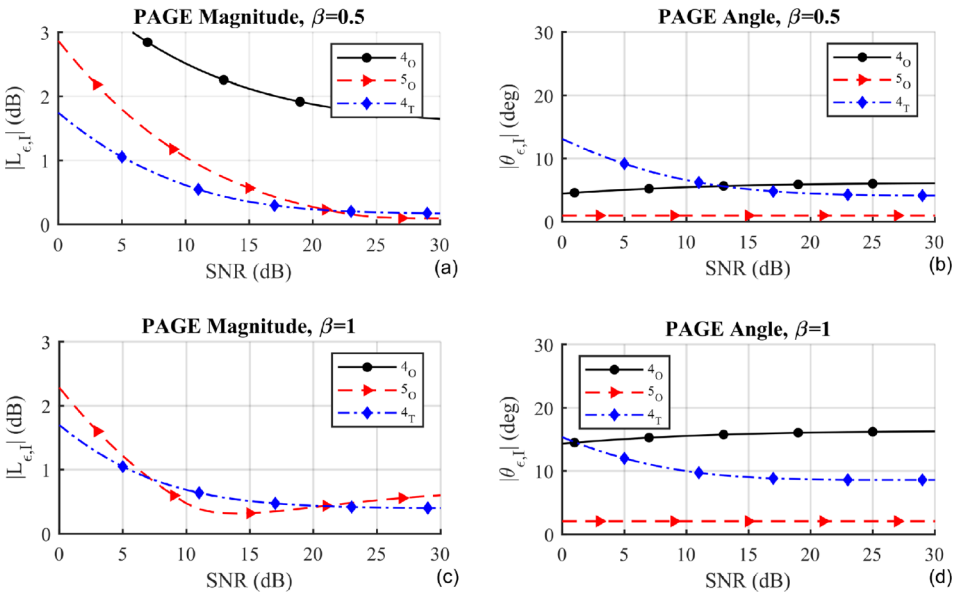


FIG. 11. (Color online) Probe comparison of bias errors for a monopole source at two distances ($\beta = 0.5$ and $\beta = 1$) with contaminating uncorrelated noise using the PAGE method. Both magnitude and direction errors are shown for both cases. In (c) the bias errors for $4_O$ are greater than 3 dB for all SNR values below 30 dB.

### B. Correlated noise

To avoid using a large number of two-dimensional plots to compare probe geometries, figures are not presented in this section; rather, simple conclusions are stated. See the tables in the appendix for further comparison of bias errors for the different probe geometries.

With the traditional method, $4_O$ and $5_O$ have essentially identical bias errors except for very near the monopole source, when the difference in microphone spacing is accounted for. $4_T$ is worse at calculating the angle for large values of $\theta_{sep}$, though the errors caused by high values of $ka$ appear later than for the other probes, and the magnitude estimation can be slightly better. Near a monopole source, all probes exhibit large magnitude errors, while the angular error varies rapidly with SNR and $ka$ for each probe configuration.

For the PAGE method, the same general trends hold for correlated noise as for uncorrelated noise. For a plane-wave source, each probe performs the same. Near a monopole source, $4_O$ exhibits greater errors than those for $5_O$, which again is a result of estimating the center pressure. With regard to the effects of separation angle, larger values of $ka$ are again less affected while lower values can show marked differences. For SNR values greater than 20 dB the bias errors are extremely low, though some errors are obtained in the extreme monopole near field, most notably for $4_O$, in which case either $4_T$ or $5_O$ performs better, depending on $\beta$ and the SNR.

## VI. CONCLUSIONS

Contaminating noise can have a great impact on the calculation of active acoustic intensity. The differences in how the traditional method and the PAGE method calculate the intensity lead to different intensity results. The PAGE method is nearly always better at computing the intensity direction, regardless of the source properties or noise type. This is because it uses the phase values of cross-spectra, and the magnitude and phase portions are separable for plane-wave signals, while for monopole sources the magnitude and phase portions are somewhat loosely intertwined. Any time the SNR exceeds about 20 dB, the bias errors using the PAGE method are small in comparison to the traditional method. With regard to magnitude, it is possible to correct for the extra measured pressure caused by uncorrelated contaminating noise; this will be investigated in future work. Near a monopole source, $5_O$ is the probe with the least bias in most cases, though for some situations $4_T$ can work better,

TABLE V. The analytical expressions for intensity bias given in orthogonal directions. Note the arguments of cross-spectra are used, though the arguments of the transfer functions are equivalent (since they differ by a factor of auto-spectra, which are always real and so do not alter the argument).

| Calculated intensity bias error components | | | |
|---|---|---|---|
| $4_O$ | $I_{\hat{x}}$ | Trad | $-\frac{\mathrm{Im}\{G_{23}\}}{2kaA_s^2}$ |
| | | PAGE | $-\frac{\left(\sqrt{G_{22}}+\sqrt{G_{33}}\right)^2 \arg\{G_{23}\}}{8kaA_s^2}$ |
| | $I_{\hat{y}}$ | Trad | $\frac{\mathrm{Im}\{G_{45}\}}{2kaA_s^2}$ |
| | | PAGE | $\frac{\left(\sqrt{G_{44}}+\sqrt{G_{55}}\right)^2 \arg\{G_{45}\}}{8kaA_s^2}$ |
| $5_O$ | $I_{\hat{x}}$ | Trad | $\frac{\mathrm{Im}\{G_{12}\}-\mathrm{Im}\{G_{13}\}}{2kaA_s^2}$ |
| | | PAGE | $-\frac{G_{11}\arg\{G_{23}\}}{2kaA_s^2}$ |
| | $I_{\hat{y}}$ | Trad | $-\frac{\mathrm{Im}\{G_{14}\}-\mathrm{Im}\{G_{15}\}}{2kaA_s^2}$ |
| | | PAGE | $\frac{G_{11}\arg\{G_{45}\}}{2kaA_s^2}$ |
| $4_T$ | $I_{\hat{x}}$ | Trad | $-\frac{\mathrm{Im}\{G_{13t}+G_{14t}-2G_{12}\}}{3kaA_s^2}$ |
| | | PAGE | $-\frac{G_{11}(\arg\{G_{24t}\}+\arg\{G_{23t}\})}{3kaA_s^2}$ |
| | $I_{\hat{y}}$ | Trad | $\frac{\mathrm{Im}\{G_{14t}-G_{13t}\}}{\sqrt{3}kaA_s^2}$ |
| | | PAGE | $\frac{G_{11}\arg\{G_{3t4t}\}}{\sqrt{3}kaA_s^2}$ |

TABLE VI. Intensity bias error components for a plane-wave source with contaminating uncorrelated noise.

| Plane-wave Source, Uncorrelated Noise | | | |
|---|---|---|---|
| $4_O$ | $I_{\hat{x}}$ | Trad | $\frac{\sin(2ka\cos\theta_s)}{2ka}$ |
| | | PAGE | $(1+10^{(-\mathrm{SNR}/10)})\cos\theta_s$ |
| | $I_{\hat{y}}$ | Trad | $\frac{\sin(2ka\sin\theta_s)}{2ka}$ |
| | | PAGE | $(1+10^{(-\mathrm{SNR}/10)})\sin\theta_s$ |
| $5_O$ | $I_{\hat{x}}$ | Trad | $\frac{\sin(ka\cos\theta_s)}{ka}$ |
| | | PAGE | $(1+10^{(-\mathrm{SNR}/10)})\cos\theta_s$ |
| | $I_{\hat{y}}$ | Trad | $\frac{\sin(ka\sin\theta_s)}{ka}$ |
| | | PAGE | $(1+10^{(-\mathrm{SNR}/10)})\sin\theta_s$ |
| $4_T$ | $I_{\hat{x}}$ | Trad | $\frac{\sin\left(\frac{1}{2}ka\cos\theta_s\right)\cos\left(\frac{\sqrt{3}}{2}ka\sin\theta_s\right)+\sin(ka\cos\theta_s)}{\frac{3}{2}ka}$ |
| | | PAGE | $(1+10^{(-\mathrm{SNR}/10)})\cos\theta_s$ |
| | $I_{\hat{y}}$ | Trad | $\frac{\cos\left(\frac{1}{2}ka\cos\theta_s\right)\sin\left(\frac{\sqrt{3}}{2}ka\sin\theta_s\right)}{\frac{\sqrt{3}}{2}ka}$ |
| | | PAGE | $(1+10^{(-\mathrm{SNR}/10)})\sin\theta_s$ |

depending on the exact values of $\beta$ and the SNR. For plane-wave sources, each probe configuration is essentially the same.

The main problem with the traditional method is its bandwidth limitation. For any large values of $ka$ (above 0.5) the bias errors are never insignificant. The magnitude and angular biases are invariably intertwined. In some cases, the magnitude and angular inaccuracies can cancel to cause smaller biases, though this is a complicated interaction. For small values of $ka$ (less than 0.5) with small SNR values (below 10–15 dB), the traditional method can sometimes better calculate the intensity magnitude. The probe that performs most consistently is $5_O$, though depending on the situation, either of the other probes can be more efficient.

Small SNR values (below 10 dB) can have adverse effects on the calculation of the PAGE method, though it is possible to correct for this, especially when the contaminating noise is uncorrelated. Angularly separated signals do not impact the PAGE method as much as the traditional method, especially for higher $ka$ values. Whenever large values of $ka$ are of interest (above 0.5), or when the SNR exceeds about 20 dB, the PAGE method gives more reliable results than the traditional method.

TABLE VII. Intensity bias error components for a monopole source with contaminating uncorrelated noise.

| Monopole Source, Uncorrelated Noise | | | |
|---|---|---|---|
| $4_O$ | $I_{\hat{x}}$ | Trad | $\frac{\sin\left(kr\sqrt{1+2\beta\cos\theta_s+\beta^2}-kr\sqrt{1-2\beta\cos\theta_s+\beta^2}\right)}{2ka\sqrt{1-2\beta^2\cos2\theta_s+\beta^4}}$ |
| | | PAGE | $\left(\frac{1}{2}\sqrt{\frac{1}{1-2\beta\cos\theta_s+\beta^2}+10^{(-\mathrm{SNR}/10)}}+\frac{1}{2}\sqrt{\frac{1}{1+2\beta\cos\theta_s+\beta^2}+10^{(-\mathrm{SNR}/10)}}\right)^2\left(\frac{1}{2\beta}\sqrt{1+2\beta\cos\theta_s+\beta^2}-\frac{1}{2\beta}\sqrt{1-2\beta\cos\theta_s+\beta^2}\right)$ |
| | $I_{\hat{y}}$ | Trad | $\frac{\sin\left(kr\sqrt{1-2\beta\sin\theta_s+\beta^2}-kr\sqrt{1+2\beta\sin\theta_s+\beta^2}\right)}{2ka\sqrt{1+2\beta^2\cos2\theta_s+\beta^4}}$ |
| | | PAGE | $\left(\frac{1}{2}\sqrt{\frac{1}{1-2\beta\sin\theta_s+\beta^2}+10^{(-\mathrm{SNR}/10)}}+\frac{1}{2}\sqrt{\frac{1}{1+2\beta\sin\theta_s+\beta^2}+10^{(-\mathrm{SNR}/10)}}\right)^2\left(\frac{1}{2\beta}\sqrt{1+2\beta\sin\theta_s+\beta^2}-\frac{1}{2\beta}\sqrt{1-2\beta\sin\theta_s+\beta^2}\right)$ |
| $5_O$ | $I_{\hat{x}}$ | Trad | $\frac{\sin\left(kr-kr\sqrt{1-2\beta\cos\theta_s+\beta^2}\right)}{2ka\sqrt{1-2\beta\cos\theta_s+\beta^2}}-\frac{\sin\left(kr-kr\sqrt{1+2\beta\cos\theta_s+\beta^2}\right)}{2ka\sqrt{1+2\beta\cos\theta_s+\beta^2}}$ |
| | | PAGE | $(1+10^{(-\mathrm{SNR}/10)})\left(\frac{1}{2\beta}\sqrt{1+2\beta\cos\theta_s+\beta^2}-\frac{1}{2\beta}\sqrt{1-2\beta\cos\theta_s+\beta^2}\right)$ |
| | $I_{\hat{y}}$ | Trad | $\frac{\sin\left(kr-kr\sqrt{1-2\beta\sin\theta_s+\beta^2}\right)}{2ka\sqrt{1-2\beta\sin\theta_s+\beta^2}}-\frac{\sin\left(kr-kr\sqrt{1+2\beta\sin\theta_s+\beta^2}\right)}{2ka\sqrt{1+2\beta\sin\theta_s+\beta^2}}$ |
| | | PAGE | $(1+10^{(-\mathrm{SNR}/10)})\left(\frac{1}{2\beta}\sqrt{1+2\beta\sin\theta_s+\beta^2}-\frac{1}{2\beta}\sqrt{1-2\beta\sin\theta_s+\beta^2}\right)$ |
| $4_T$ | $I_{\hat{x}}$ | Trad | $\frac{\sin\left(kr-kr\sqrt{1-2\beta\cos\theta_s+\beta^2}\right)}{\frac{3}{2}ka\sqrt{1-2\beta\cos\theta_s+\beta^2}}+\frac{\sin\left(\frac{1}{2}ka\cos\theta_s+\frac{\sqrt{3}}{2}ka\sin\theta_s\right)}{3ka+3\beta\left(\frac{1}{2}ka\cos\theta_s+\frac{\sqrt{3}}{2}ka\sin\theta_s\right)}-\frac{\sin\left(\frac{1}{2}ka\cos\theta_s-\frac{\sqrt{3}}{2}ka\sin\theta_s\right)}{3ka+3\beta\left(\frac{1}{2}ka\cos\theta_s-\frac{\sqrt{3}}{2}ka\sin\theta_s\right)}$ |
| | | PAGE | $(1+10^{(-\mathrm{SNR}/10)})\left(\frac{1}{3}\cos\theta_s+\frac{2}{3\beta}\left(1-\sqrt{1-2\beta\cos\theta_s+\beta^2}\right)\right)$ |
| | $I_{\hat{y}}$ | Trad | $\frac{\sin\left(\frac{1}{2}ka\cos\theta_s+\frac{\sqrt{3}}{2}ka\sin\theta_s\right)}{\sqrt{3}ka+\sqrt{3}\beta\left(\frac{1}{2}ka\cos\theta_s+\frac{\sqrt{3}}{2}ka\sin\theta_s\right)}-\frac{\sin\left(\frac{1}{2}ka\cos\theta_s-\frac{\sqrt{3}}{2}ka\sin\theta_s\right)}{\sqrt{3}ka+\sqrt{3}\beta\left(\frac{1}{2}ka\cos\theta_s-\frac{\sqrt{3}}{2}ka\sin\theta_s\right)}$ |
| | | PAGE | $(1+10^{(-\mathrm{SNR}/10)})\sin\theta_s$ |

TABLE VIII. Intensity bias error components for a plane-wave source with contaminating plane-wave noise.

| Plane-wave Source, Plane-wave Noise | | | |
|---|---|---|---|
| $4_O$ | $I_{\hat{x}}$ | Trad | $\frac{\sin(2ka\cos\theta_s)}{2ka} + 10^{(-\mathrm{SNR}/10)}\frac{\sin(2ka\cos\theta_n)}{2ka}$ |
| | | PAGE | $(1+10^{(-\mathrm{SNR}/10)})\frac{1}{2ka}\arg\left\{e^{2jka\cos\theta_s} + 10^{(-\mathrm{SNR}/10)}e^{2jka\cos\theta_n}\right\}$ |
| | $I_{\hat{y}}$ | Trad | $\frac{\sin(2ka\sin\theta_s)}{2ka} + 10^{(-\mathrm{SNR}/10)}\frac{\sin(2ka\sin\theta_n)}{2ka}$ |
| | | PAGE | $(1+10^{(-\mathrm{SNR}/10)})\frac{1}{2ka}\arg\left\{e^{2jka\sin\theta_s} + 10^{(-\mathrm{SNR}/10)}e^{2jka\sin\theta_n}\right\}$ |
| $5_O$ | $I_{\hat{x}}$ | Trad | $\frac{\sin(ka\cos\theta_s)}{ka} + 10^{(-\mathrm{SNR}/10)}\frac{\sin(ka\cos\theta_n)}{ka}$ |
| | | PAGE | $(1+10^{(-\mathrm{SNR}/10)})\frac{1}{2ka}\arg\left\{e^{2jka\cos\theta_s} + 10^{(-\mathrm{SNR}/10)}e^{2jka\cos\theta_n}\right\}$ |
| | $I_{\hat{y}}$ | Trad | $\frac{\sin(ka\sin\theta_s)}{ka} + 10^{(-\mathrm{SNR}/10)}\frac{\sin(ka\sin\theta_n)}{ka}$ |
| | | PAGE | $(1+10^{(-\mathrm{SNR}/10)})\frac{1}{2ka}\arg\left\{e^{2jka\sin\theta_s} + 10^{(-\mathrm{SNR}/10)}e^{2jka\sin\theta_n}\right\}$ |
| $4_T$ | $I_{\hat{x}}$ | Trad | $\frac{\sin\left(\frac{1}{2}ka\cos\theta_s\right)\cos\left(\frac{\sqrt{3}}{2}ka\sin\theta_s\right)+\sin(ka\cos\theta_s)}{\frac{3}{2}ka} + 10^{(-\mathrm{SNR}/10)}\frac{\sin\left(\frac{1}{2}ka\cos\theta_n\right)\cos\left(\frac{\sqrt{3}}{2}ka\sin\theta_n\right)+\sin(ka\cos\theta_n)}{\frac{3}{2}ka}$ |
| | | PAGE | $(1+10^{(-\mathrm{SNR}/10)})\left(\frac{1}{3ka}\arg\left\{e^{j\left((3/2)ka\cos\theta_s-(\sqrt{3}/2)ka\sin\theta_s\right)} + 10^{(-\mathrm{SNR}/10)}e^{j\left((3/2)ka\cos\theta_n-(\sqrt{3}/2)ka\sin\theta_n\right)}\right\}\right.$ $\left.+\frac{1}{3ka}\arg\left\{e^{j\left((3/2)ka\cos\theta_s+(\sqrt{3}/2)ka\sin\theta_s\right)} + 10^{(-\mathrm{SNR}/10)}e^{j\left((3/2)ka\cos\theta_n+(\sqrt{3}/2)ka\sin\theta_n\right)}\right\}\right)$ |
| | $I_{\hat{y}}$ | Trad | $\frac{\cos\left(\frac{1}{2}ka\cos\theta_s\right)\sin\left(\frac{\sqrt{3}}{2}ka\sin\theta_s\right)}{\frac{\sqrt{3}}{2}ka} + 10^{(-\mathrm{SNR}/10)}\frac{\cos\left(\frac{1}{2}ka\cos\theta_n\right)\sin\left(\frac{\sqrt{3}}{2}ka\sin\theta_n\right)}{\frac{\sqrt{3}}{2}ka}$ |
| | | PAGE | $(1+10^{(-\mathrm{SNR}/10)})\frac{1}{\sqrt{3}ka}\arg\left\{e^{\sqrt{3}jka\sin\theta_s} + 10^{(-\mathrm{SNR}/10)}e^{\sqrt{3}jka\sin\theta_n}\right\}$ |


## ACKNOWLEDGMENTS

This work was funded by the National Science Foundation, Grant No. 1538550, "Developing New Methods for Obtaining Energy-based Acoustic Quantities."


## APPENDIX

Equation tables are included herein. Table V gives the equations for how the orthogonal components of the intensity bias errors, $I_{\hat{x}}$ and $I_{\hat{y}}$, are calculated for the different probe configurations, using the auto- and cross-spectral values. Tables VI–IX give the simplified intensity bias components for plane-wave and monopole sources with uncorrelated and self-correlated contaminating noise. In each case, perfect calculation would yield $I_{\hat{x}} = \cos\theta_s$ and $I_{\hat{y}} = \sin\theta_s$. The magnitude and angular biases are given by $L_{\epsilon,\boldsymbol{I}} = 10\log_{10}\left(\sqrt{I_{\hat{x}}^2+I_{\hat{y}}^2}\right) = 5\log_{10}(I_{\hat{x}}^2+I_{\hat{y}}^2)$ and $\theta_{\epsilon,\boldsymbol{I}} = \tan^{-1}(I_{\hat{y}}/I_{\hat{x}}) - \theta_s$.

TABLE IX. Intensity bias error components for a monopole source with contaminating plane-wave noise.

| Monopole Source, Plane-wave Noise | | | |
|---|---|---|---|
| $4_O$ | $I_{\hat{x}}$ | Trad | $\frac{\sin\left(kr\sqrt{1+2\beta\cos\theta_s+\beta^2}-kr\sqrt{1-2\beta\cos\theta_s+\beta^2}\right)}{2ka\sqrt{1-2\beta^2\cos2\theta_s+\beta^4}} + 10^{(-\mathrm{SNR}/10)}\frac{\sin(2ka\cos\theta_n)}{2ka}$ |
| | | PAGE | $\left(\frac{1}{2}\sqrt{\frac{1}{1-2\beta\cos\theta_s+\beta^2}+10^{(-\mathrm{SNR}/10)}}+\frac{1}{2}\sqrt{\frac{1}{1+2\beta\cos\theta_s+\beta^2}+10^{(-\mathrm{SNR}/10)}}\right)^2$ $\times\left(\frac{1}{2ka}\arg\left\{e^{jkr\left(\sqrt{1+2\beta\cos\theta_s+\beta^2}-\sqrt{1-2\beta\cos\theta_s+\beta^2}\right)} + 10^{(-\mathrm{SNR}/10)}\sqrt{1-2\beta^2\cos2\theta_s+\beta^4}e^{2jka\cos\theta_n}\right\}\right)$ |
| | $I_{\hat{y}}$ | Trad | $\frac{\sin\left(kr\sqrt{1-2\beta\sin\theta_s+\beta^2}-kr\sqrt{1+2\beta\sin\theta_s+\beta^2}\right)}{2ka\sqrt{1+2\beta^2\cos2\theta_s+\beta^4}} + 10^{(-\mathrm{SNR}/10)}\frac{\sin(2ka\sin\theta_n)}{2ka}$ |
| | | PAGE | $\left(\frac{1}{2}\sqrt{\frac{1}{1-2\beta\sin\theta_s+\beta^2}+10^{(-\mathrm{SNR}/10)}}+\frac{1}{2}\sqrt{\frac{1}{1+2\beta\sin\theta_s+\beta^2}+10^{(-\mathrm{SNR}/10)}}\right)^2\left(\frac{1}{2ka}\arg\left\{e^{jkr\left(\sqrt{1+2\beta\sin\theta_s+\beta^2}-\sqrt{1-2\beta\sin\theta_s+\beta^2}\right)}\right.\right.$ $\left.\left.+10^{(-\mathrm{SNR}/10)}\sqrt{1+2\beta^2\cos2\theta_s+\beta^4}e^{2jka\sin\theta_n}\right\}\right)$ |

TABLE IX. (*Continued*)

Monopole Source, Plane-wave Noise

| | | | |
|---|---|---|---|
| $5_O$ | $I_{\hat{x}}$ | Trad | $\frac{\sin\left(kr-kr\sqrt{1-2\beta\cos\theta_s+\beta^2}\right)}{2ka\sqrt{1-2\beta\cos\theta_s+\beta^2}}-\frac{\sin\left(kr-kr\sqrt{1+2\beta\cos\theta_s+\beta^2}\right)}{2ka\sqrt{1+2\beta\cos\theta_s+\beta^2}}+10^{(-\mathrm{SNR}/10)}\frac{\sin(ka\cos\theta_n)}{ka}$ |
| | | PAGE | $(1+10^{(-\mathrm{SNR}/10)})\left(\frac{1}{2ka}\arg\left\{e^{jkr\left(\sqrt{1+2\beta\cos\theta_s+\beta^2}-\sqrt{1-2\beta\cos\theta_s+\beta^2}\right)}+10^{(-\mathrm{SNR}/10)}\sqrt{1-2\beta^2\cos 2\theta_s+\beta^4}e^{2jka\cos\theta_n}\right\}\right)$ |
| | $I_{\hat{y}}$ | Trad | $\frac{\sin\left(kr-kr\sqrt{1-2\beta\sin\theta_s+\beta^2}\right)}{2ka\sqrt{1-2\beta\sin\theta_s+\beta^2}}-\frac{\sin\left(kr-kr\sqrt{1+2\beta\sin\theta_s+\beta^2}\right)}{2ka\sqrt{1}}+2\beta\sin\theta_s+\beta^2+10^{(-\mathrm{SNR}/10)}\frac{\sin(ka\sin\theta_n)}{ka}$ |
| | | PAGE | $(1+10^{(-\mathrm{SNR}/10)})\left(\frac{1}{2ka}\arg\left\{e^{jkr\left(\sqrt{1+2\beta\sin\theta_s+\beta^2}-\sqrt{1-2\beta\sin\theta_s+\beta^2}\right)}+10^{(-\mathrm{SNR}/10)}\sqrt{1+2\beta^2\cos 2\theta_s+\beta^4}e^{2jka\sin\theta_n}\right\}\right)$ |
| $4_T$ | $I_{\hat{x}}$ | Trad | $\frac{\sin\left(kr-kr\sqrt{1-2\beta\cos\theta_s+\beta^2}\right)}{\frac{3}{2}ka\sqrt{1-2\beta\cos\theta_s+\beta^2}}+\frac{\sin\left(\frac{1}{2}ka\cos\theta_s+\frac{\sqrt{3}}{2}ka\sin\theta_s\right)}{3ka+3\beta\left(\frac{1}{2}ka\cos\theta_s+\frac{\sqrt{3}}{2}ka\sin\theta_s\right)}-\frac{\sin\left(\frac{1}{2}ka\cos\theta_s-\frac{\sqrt{3}}{2}ka\sin\theta_s\right)}{3ka+3\beta\left(\frac{1}{2}ka\cos\theta_s-\frac{\sqrt{3}}{2}ka\sin\theta_s\right)}+10^{(-\mathrm{SNR}/10)}\frac{\sin\left(\frac{1}{2}ka\cos\theta_n\right)\cos\left(\frac{\sqrt{3}}{2}ka\sin\theta_n\right)+\sin(ka\cos\theta_n)}{\frac{3}{2}ka}$ |
| | | PAGE | $(1+10^{(-\mathrm{SNR}/10)})\left(\frac{1}{3ka}\arg\left\{e^{j\left(kr-kr\sqrt{1-2\beta\cos\theta_s+\beta^2}+(1/2)ka\cos\theta_s-(\sqrt{3}/2)ka\sin\theta_s\right)}+10^{(-\mathrm{SNR}/10)}\sqrt{1-2\beta\cos\theta_s+\beta^2}\left(1+\frac{1}{2}\beta\cos\theta_s-\frac{\sqrt{3}}{2}\beta\sin\theta_s\right)e^{j\left((3/2)ka\cos\theta_n-(\sqrt{3}/2)ka\sin\theta_n\right)}\right\}+\frac{1}{3ka}\arg\left\{e^{j\left(kr-kr\sqrt{1-2\beta\cos\theta_s+\beta^2}+(1/2)ka\cos\theta_s+(\sqrt{3}/2)ka\sin\theta_s\right)}+10^{(-\mathrm{SNR}/10)}\sqrt{1-2\beta\cos\theta_s+\beta^2}\left(1+\frac{1}{2}\beta\cos\theta_s+\frac{\sqrt{3}}{2}\beta\sin\theta_s\right)e^{j\left((3/2)ka\cos\theta_n-(\sqrt{3}/2)ka\sin\theta_n\right)}\right\}\right)$ |
| | $I_{\hat{y}}$ | Trad | $\frac{\sin\left(\frac{1}{2}ka\cos\theta_s+\frac{\sqrt{3}}{2}ka\sin\theta_s\right)}{\sqrt{3}ka+\sqrt{3}\beta\left(\frac{1}{2}ka\cos\theta_s+\frac{\sqrt{3}}{2}ka\sin\theta_s\right)}-\frac{\sin\left(\frac{1}{2}ka\cos\theta_s-\frac{\sqrt{3}}{2}ka\sin\theta_s\right)}{\sqrt{3}ka+\sqrt{3}\beta\left(\frac{1}{2}ka\cos\theta_s-\frac{\sqrt{3}}{2}ka\sin\theta_s\right)}+10^{(-\mathrm{SNR}/10)}\frac{\cos\left(\frac{1}{2}ka\cos\theta_n\right)\sin\left(\frac{\sqrt{3}}{2}ka\sin\theta_n\right)}{\frac{\sqrt{3}}{2}ka}$ |
| | | PAGE | $\left(1+10^{(-\mathrm{SNR}/10)}\right)\left(\frac{1}{\sqrt{3}ka}\arg\left\{e^{\sqrt{3}jka\sin\theta_s}+10^{(-\mathrm{SNR}/10)}\left(1+\beta\cos\theta_s+\frac{1}{2}\beta^2\cos 2\theta_s-\frac{1}{4}\beta^2\right)e^{\sqrt{3}jka\sin\theta_n}\right\}\right)$ |


[1]F. J. Fahy, *Sound Intensity* (Spon, London, 1995), pp. 1–295.
[2]F. J. Fahy, "Measurement of acoustic intensity using the cross-spectral density of two microphone signals," J. Acoust. Soc. Am. **62**, 1057–1059 (1977).
[3]M. J. Crocker, "Measurement of sound intensity," in *Handbook of Acoustical Measurements and Noise Control* (McGraw-Hill, New York, 1991), pp. 14.1–14.17.
[4]J. Y. Chung, "Cross-spectral method of measuring acoustic intensity without error caused by instrument phase mismatch," J. Acoust. Soc. Am. **64**, 1613–1616 (1978).
[5]D. C. Thomas, B. Y. Christensen, and K. L. Gee, "Phase and amplitude gradient method for the estimation of acoustic vector quantities," J. Acoust. Soc. Am. **137**, 3366–3376 (2015).
[6]D. K. Torrie, E. B. Whiting, K. L. Gee, T. B. Neilsen, and S. D. Sommerfeldt, "Initial laboratory experiments to validate a phase and amplitude gradient estimator method for the calculation of acoustic intensity," Proc. Mtgs. Acoust. **23**, 030005 (2015).
[7]J. A. Mann III and J. Tichy, "Acoustic intensity analysis: Distinguishing energy propagation and wave-front propagation," J. Acoust. Soc. Am. **90**, 20–25 (1991).
[8]E. B. Whiting, J. S. Lawrence, K. L. Gee, T. B. Neilsen, and S. D. Sommerfeldt, "Bias error analysis for phase and amplitude gradient estimation of acoustic intensity and specific acoustic impedance," J. Acoust. Soc. Am. **142**, 2208–2218 (2017).
[9]E. B. Whiting, "Energy quantity estimation in radiated acoustic fields," MS thesis, Brigham Young University, 2016.
[10]J. S. Lawrence, E. B. Whiting, K. L. Gee, R. D. Rasband, T. B. Neilsen, and S. D. Sommerfeldt, "Three-microphone probe bias error for acoustic intensity and specific acoustic impedance," J. Acoust. Soc. Am. **143**, EL81–EL86 (2018).
[11]M. R. Cook, K. L. Gee, S. D. Sommerfeldt, and T. B. Neilsen, "Coherence-based phase unwrapping for broadband acoustic signals," Proc. Mtgs. Acoust. **30**, 055005 (2017).
[12]J. S. Bendat and A. G. Piersol, *Random Data: Analysis and Measurement Procedures* (Wiley, Hoboken, NJ, 2010).
[13]C. H. Oppenheimer, "A statistical background noise correction sensitive to the steadiness of background noise," J. Acoust. Soc. Am. **140**, 2888–2922 (2016).
[14]E. Y. Lo and M. C. Junger, "Signal-to-noise enhancement by underwater intensity measurements," J. Acoust. Soc. Am. **82**, 1450–1453 (1987).
[15]J. S. Lawrence, K. L. Gee, T. B. Neilsen, and S. D. Sommerfeldt, "Higher-order estimation of active and reactive acoustic intensity," Proc. Mtgs. Acoust. **30**, 055004 (2017).
[16]L. S. Goodfriend, "Correction chart for background noise," Noise Control **4**(3), 56 (1958).
[17]S. E. Bard, "A study of background noise variability in acoustical measurement laboratories," J. Acoust. Soc. Am. **132**, 2086 (2012).
[18]C. H. Oppenheimer, "An alternate background noise correction sensitive to the steadiness of background noise," ECMA TR/107 (2015).